Surface treatment of Ti–6Al–4V alloy by rf plasma nitriding

2007 J. Phys.: Condens. Matter 19 396003

(http://iopscience.iop.org/0953-8984/19/39/396003)

IOP PUBLISHING JOURNAL OF PHYSICS: CONDENSED MATTER

J. Phys.: Condens. Matter **19** (2007) 396003 (12pp) doi:10.1088/0953-8984/19/39/396003

Surface treatment of Ti–6Al–4V alloy by rf plasma nitriding

M Raaif[1,2,3], F M El-Hossary[1], N Z Negm[1], S M Khalil[1] and P Schaaf[2]

[1] Physics Department, Faculty of Science, Sohag University, Sohag, Egypt
[2] II. Physikalisches Institut, University of Göttingen, Friedrich-Hund-Platz 1, 37077 Göttingen, Germany

E-mail: raief_2001@yahoo.com

Received 5 June 2007, in final form 25 July 2007
Published 3 September 2007
Online at stacks.iop.org/JPhysCM/19/396003

Abstract

The Ti–6Al–4V alloy was treated by inductively coupled rf plasma nitriding. The effects of plasma-processing time in the range of 5–35 min on the microstructure and the mechanical properties of the plasma-nitrided Ti–6Al–4V samples were studied. The plasma power input was adjusted at 450 W and pure N_2 gas was introduced to establish a treatment pressure of 8.0–8.4 $\times$ 10^{-2} mbar. The characteristics of the nitrided layers have been investigated by microhardness testing, surface roughness measurements, optical microscopy, and x-ray diffraction. The results show that the surface microhardness increases as the plasma-processing time increases to reach 2000 HV0.1 at a plasma-processing time of 35 min. A high nitriding rate of 2.81 $\mu m^2\ s^{-1}$ at a plasma-processing time of 25 min was achieved. The formation of the hard phases TiN, Ti_2N, and Ti(N) in the Ti–6Al–4V surfaces are found to be the reason for the increased microhardness. Surface energy, yield strength and Young's modulus for the nitrided Ti–6Al–4V alloy were calculated from the Vickers microhardness data.

(Some figures in this article are in colour only in the electronic version)

1. Introduction

Ti–6Al–4V alloy has frequently been used for orthopedic devices and other engineering components due to its beneficial properties, such as low density, low modulus of elasticity, excellent corrosion resistance and biocompatibility [1]. However, the inadequate wear behavior of Ti–6Al–4V alloy has limited its use in many applications. For example, numerous engineering components made of Ti–6Al–4V alloy are easily damaged at the surfaces in contact under load and in relative motion [2, 3]. Nitriding is proposed as a process to

[3] Author to whom any correspondence should be addressed.

improve the surface properties. The diffusion of nitrogen into the bulk material produces a continuous hardness profile and therefore provides optimal support of the hard surface layer. This surface layer is normally composed of the face centered cubic δ-TiN and tetragonal ε-Ti_2N phases [4]. Moreover, the outermost δ-TiN layer is known to be wear [5] and corrosion resistant [6] and biocompatible [7, 8]. Conventional treatments require high temperatures [9], which lead to severe structural modifications that deteriorate the mechanical properties. Plasma nitriding and especially (rf) plasma nitriding is one of the most effective processes at low temperature, avoiding modifications of the microstructure and of the mechanical properties of the bulk [10–12]. Moreover, plasma nitriding allows an homogeneous treatment of the entire surface, even of complex shapes (like biomedical implant pieces), thus reducing the treatment costs of such costly parts [4].

The present study was planned with the aim of enhancing the microstructure and mechanical properties of the Ti–6Al–4V alloy surface by using rf plasma nitriding and thus forming TiN, Ti_2N and Ti(N) superhard phases. Achieving a hard surface with high efficiency by means of a nitriding process using different plasma-processing times was the main task. The properties and characteristics of the processed samples are evaluated using Vickers microhardness test (HV), optical microscopy, surface roughness measurements, and x-ray diffraction. The surface energy, yield strength and elastic modulus for nitrided Ti–6Al–4V were also calculated from Vickers microhardness data.

2. Experimental details

The as-received Ti–6Al–4V bars were cut into discs of approximately 1.5–2 mm thickness and 1 cm in diameter. They were ground and polished to give an initial surface roughness of $R_a = 0.06\ \mu$m. The nitriding process was established using an rf inductively coupled glow discharge with a continuous mode of operation. Details of the nitriding system can be found in [13]. In brief, the system comprises a quartz reactor with a 500 mm long tube of 41.5 mm diameter, which was evacuated to a base pressure of 2 Pa by a two-stage rotary pump. The Ti–6Al–4V samples are located in the middle of the rf external copper coil and supported by a 2.9 cm long titanium bar with a diameter of 1 cm. These are fixed on a water-cooled copper sample holder. Nitrogen gas (N_2) was introduced to establish a gas pressure of 8.4 Pa and measured by means of a capacitance manometer. The induction copper coil, energized by an rf power generator model HFS 2500 D at 13.65 MHz via a tunable matching network, generated the discharge. The sample temperature was measured during the rf plasma process by a Chromel–Alumel thermocouple, which was placed close to the surface of the sample. After the nitriding process, the samples were allowed to cool slowly in the evacuated reactor plasma tube. The plasma power input was fixed at 450 W and all the other plasma parameters were fixed except the plasma-processing time, which was varied from 5 up to 35 min in steps of 5 min. There was no auxiliary heating source for heating the samples.

X-ray diffraction (XRD) analyses of the nitrided surface were performed using a Philips x-ray diffractometer. The patterns of the x-ray diffraction analysis were run in a normal θ–2θ scan between 30° and 100°, with step intervals of 0.02°. Cu Kα radiation with an average wavelength λ of 1.540 56 Å was used. The step time was adjusted to be 0.5 s and the temperature was 27 °C. Vickers microhardness measurements were carried out for the nitrided surfaces using a microhardness tester with a contact load of 100 g for a peak-load contact of 15 s. The surface roughness was measured using a Dektak3ST surface profiler measuring system. The cross-section morphology of treated titanium alloy samples were investigated using an optical microscope. The treated samples were cross sectioned and cold embedded in epoxy material. Grinding of the samples was performed using water-proof silicon

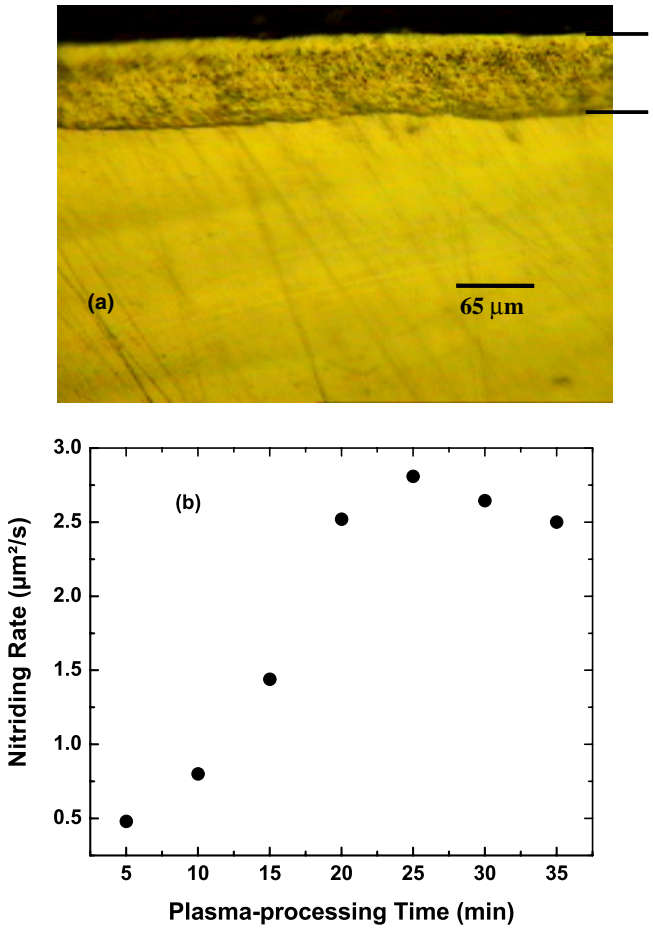

Figure 1. (a) Optical micrograph of a Ti–6Al–4V sample treated for a plasma-processing time of 25 min. (b) Nitriding rate as a function of the plasma-processing time.

carbide paper FEAP P(120–4000) followed by polishing using alumina suspensions 0.3 and 0.1. Moreover, the etching process performed by using 100 ml H_2O + 50 ml ethanol + 2 g ammonium hydrogen fluoride with times from seconds to minute. Finally, the samples were washed and swabbed in warm running water. A micrometer scale attached to the optical microscope measures the thickness of treated layer.

3. Results and discussion

3.1. Microstructure of the nitrided layers of Ti–6Al–4V alloy

Figure 1(a) shows a typical optical cross-section of an rf plasma nitrided sample which was treated for a plasma-processing time of 25 min. This figure shows that the compound layer has an homogeneous band of nearly uniform thickness and a sharp edge with the bulk. The variation of the parabolic nitriding rate, ($\mu m^2\ s^{-1}$), as a function of the plasma-processing time is shown in figure 1(b). It can be seen that the nitriding rate increases with the plasma-processing time up to 25 min. With a further increase in the plasma-processing time, the rate gradually decreases.

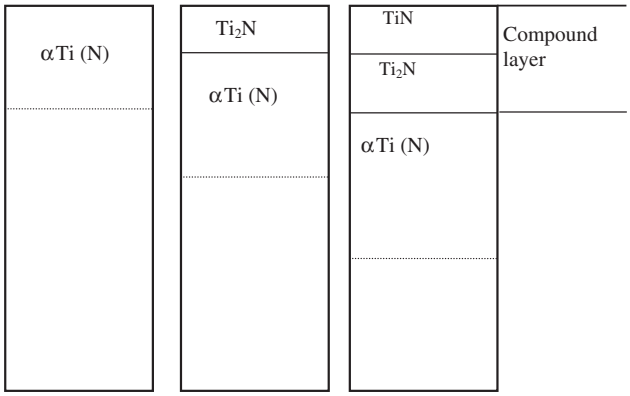

Figure 2. A schematic presentation of the kinetics of formation and growth of surface layers during nitriding of titanium.

The formation of nitrided layers in titanium alloys is a complicated process and involves several reactions taking place simultaneously at the boundary between the gas and the metal. The kinetics of the diffusion process has been studied by several research groups [14–17]. A simplified physical model for the formation and growth of nitrided layers during gas nitriding in titanium has been suggested by [18]. The model is based on the reaction diffusion rules and it is applicable for nitriding temperatures below the β-transition ($\alpha \rightarrow \beta$ transition temperature). If the titanium material is in an active nitrogen-containing environment at high temperature, a nitrogen mass transfer from the medium to the solid occurs. The nitrogen absorbed at the surface diffuses into the titanium, forming an interstitial solution of nitrogen in the (hcp) α-titanium phase (figure 2 left). The surface layer formed is called the diffusion zone (α(N)). This process can continue as long as the α-titanium matrix can dissolve nitrogen at the nitrogen medium/solid interface. If the concentration of nitrogen at the gas/metal interface becomes higher than the solubility in the α-phase, a reaction at the interface occurs, leading to the formation of a new phase, Ti_2N (figure 2 middle). There is a jump in concentration of nitrogen at the sample surface and, as a result, the total nitrided layer consists of a compound layer (Ti_2N) on the top and a diffusion zone underneath. Following the same rules, when the concentration of nitrogen at the gas/metal interface becomes higher than the one acceptable in Ti_2N, there is a phase transformation at the sample surface and the Ti_2N transforms to TiN (figure 2 right). The sublayer with titanium nitrides only (TiN and Ti_2N) forms the compound layer, while α(N) is the diffusion zone. The sequence of phase transitions at the sample surface during nitriding can be written as:

$$\alpha - \mathrm{Ti} \Rightarrow \alpha(\mathrm{N}) - \mathrm{Ti} \Rightarrow \mathrm{Ti_2N} \Rightarrow \mathrm{TiN}. \tag{1}$$

The evolution of the surface layer during nitriding is presented schematically in figure 2. This mechanism is insufficient to interpret the high value of nitriding rate that we have obtained here. Therefore, we have adapted the formed microcracks mechanism reported by El-Hossary [19], together with the diffusion mechanism. At a certain temperature, depending on the treated material, and at a high nitrogen concentration and a high plasma energy, the chance of surface microcracks and a high penetration of the nitrogen species occurring is high. The nitrogen diffuses into the native material through the sample surface (mainly through the grain boundaries) and the wall of the formed microcracks, in which the interface in between (treated and native titanium alloy) is large enough for a fast nitriding process due to the concentration gradient. The diffusion of nitrogen in titanium alloy might be due to an interstitial or vacancy

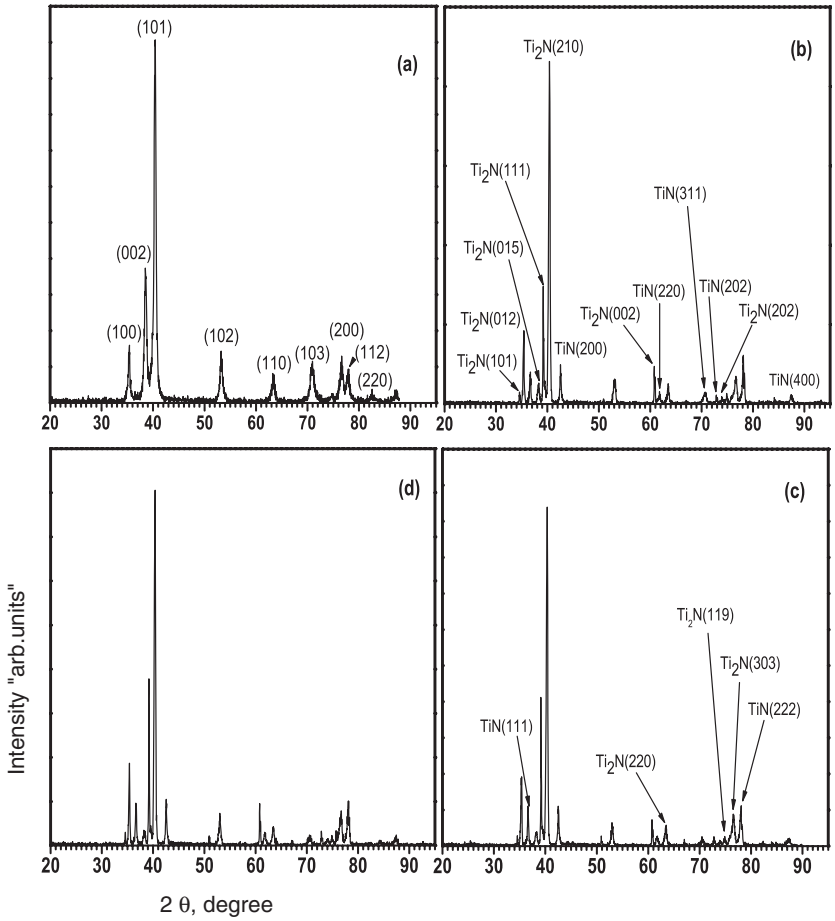

Figure 3. X-ray diffraction patterns for untreated Ti–6Al–4V sample (a) and treated Ti–6Al–4V samples for plasma-processing times of: (b) 20 min, (c) 25 min and (d) 35 min.

mechanism, depending on the sample temperature. After a certain duration of plasma operation, the nitrided phases might block the previously formed microcracks in the compound layer. Therefore, the penetration of the nitrogen species rate through these microcracks decreases.

The main phases can be observed on the surface of Ti–6Al–4V, after plasma nitriding, are ε-Ti_2N, δ-TiN, and α-Ti(N). Figure 3 shows the typical x-ray diffraction patterns for the untreated and treated Ti–6Al–4V samples at different plasma-processing times of 20, 25, and 35 min. Moreover, the x-ray diffraction data for the sample that was treated for a plasma-processing time of 20 min is indexed, as shown in table 1.

Figure 3(a) displays the XRD pattern for the as-received Ti–6Al–4V sample. One can see from the diffraction pattern that the peaks are assigned to the hexagonal α-Ti and cubic β-Ti phases [20]. The β-Ti phase is clearly characterized by the (110) and (200) reflections. As a consequence of the α structure, Ti–6Al–4V shows prismatic and pyramidal slip systems, which cause relatively low shear strength and high friction coefficients [21]. As the plasma-processing time increases, new hard phases are formed, as seen in figures 3(b)–(d). This figure clarifies that the most intense peaks are assigned to ε-Ti_2N, δ-TiN, and α-Ti(N). According to [4, 22, 23], δ and ε-phases are expected to be the reason for the high values of the microhardness of the

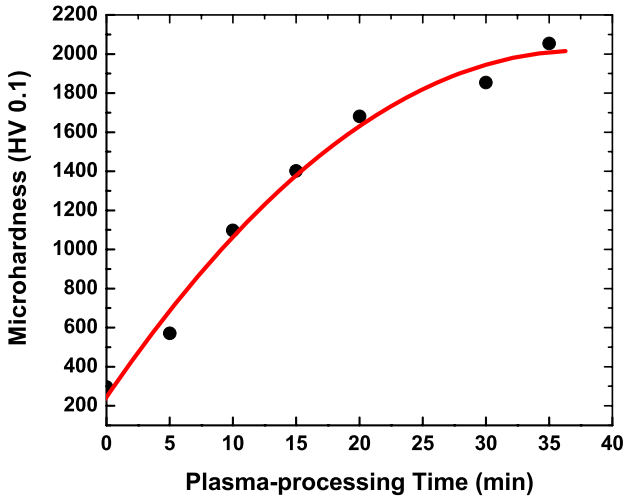

Figure 4. Microhardness values of untreated and treated Ti–6Al–4V samples at different plasma-processing times.

Table 1. X-ray diffraction data for the sample which was treated for a plasma-processing time of 20 min.

2θ (grad)	d value (Å)	I (%)	Phase	hkl	Reference
34.640 01	2.587 3	2.72	Ti_2N	101	[38]
35.359 61	2.363 4	21.18	Ti_4N_{3-x} (Ti_2N)	012	[39]
36.685 32	2.447 67	8.36	TiN	111	[40]
38.347 58	2.345 31	4.39	Ti_4N_{3-x} (Ti_2N)	015	[39]
39.173 41	2.297 75	33.28	Ti_2N	111	[38]
40.972 1	2.211	100	Ti_2N	210	[38]
42.576 77	2.121 62	7.49	TiN	200	[41]
60.989 93	1.517 90	10.72	Ti_2N	002	[38]
61.814 62	1.499 62	2.32	TiN	220	[40]
63.479 39	1.464 24	4.49	Ti_2N	220	[42]
70.781 93	1.330 01	2.53	TiN	311	[43]
73.111 00	1.293 2	1.32	Ti_2N	202	[38]
74.919 39	1.266 48	2.43	Ti_3N_{2-x} (Ti_2N)	119	[44]
76.725 78	1.241 1	6.88	Ti_2N	303	[42]
78.117 00	1.222 45	14.01	TiN	222	[41]
87.517 85	1.113 72	1.48	TiN	400	[43]

nitrided Ti alloy. Moreover, a δ-TiN layer is known to be wear [5] and corrosion resistant [6] and biocompatible [7, 8].

3.2. Microhardness measurements

The microhardness values of the untreated and treated Ti–6Al–4V samples are shown in figure 4. One can see from this figure that, as the plasma treatment time increases, higher hardness values are obtained. Even for the sample that was treated for only 5 min, a microhardness value of more than 550 HV0.1 was obtained. The microhardness had a maximum value of approximately 2000 HV0.1 for the sample that was treated for a plasma-processing time of 35 min.

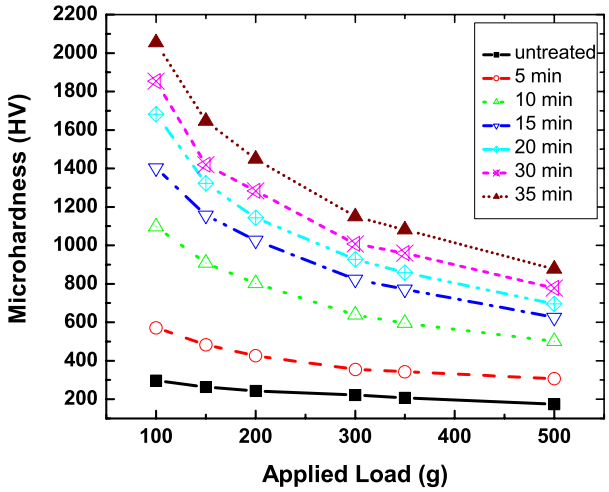

Figure 5. Microhardness values of the untreated and treated Ti–6Al–4V samples as a function of the applied loads at different plasma-processing times.

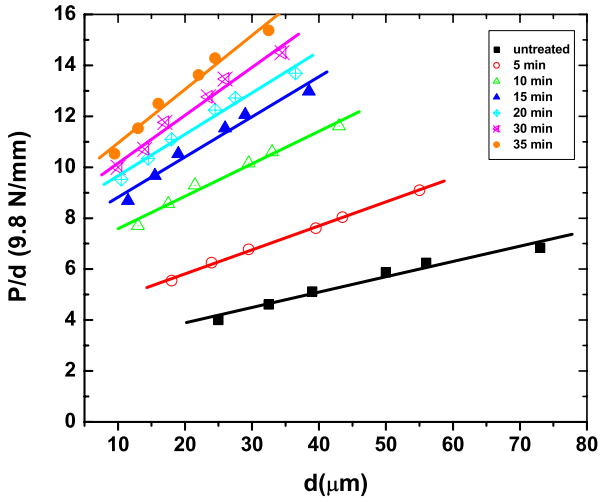

Figure 6. The variation of the ratio between the applied load and the diagonal of the impression of the untreated and treated Ti–6Al–4V samples at different plasma-processing times.

In order to accomplish the microhardness measurements, the microhardness profile of the compound layer was produced for different levels, using different loads of 100, 150, 200, 300, 350, and 500 g. Figure 5 shows the microhardness values of the untreated and the treated Ti–6Al–4V samples for different plasma-processing times as a function of the applied loads. One can observe that the microhardness values decrease with increasing applied loads for all the treated samples. This result agrees with Kawata *et al* [24].

The surface energy of a solid is defined as the excess energy of a free surface compared to that of the bulk. The determination of the surface energy of a solid is essential when considering surface properties in the areas of wetting/adhesion, friction/lubrication, and surface modification. The experimental results showe that the diagonal length of the indentation d (in μm) is strongly dependent on the load P (in N) employed for indentation. Figure 6 displays the

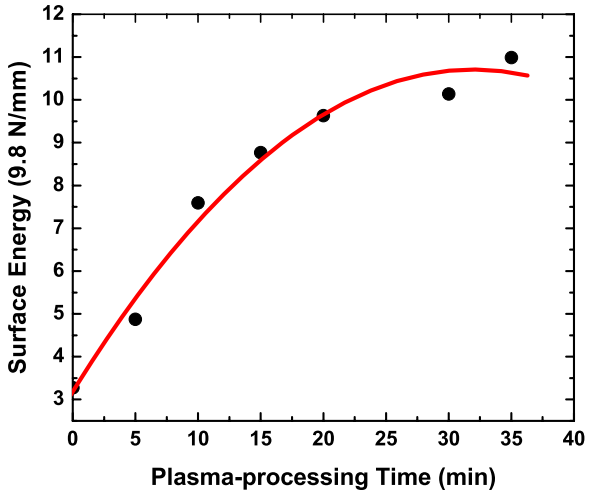

Figure 7. The surface energy as a function of the plasma-processing time.

values of P/d versus d for the untreated and treated Ti–6Al–4V samples at different plasma-processing times. A linear relationship has been observed for each sample. This result agrees well with Leenders *et al* and Veerender *et al* [25, 26]. However, this result is governed by the empirical formula: $P/d = \mathbf{A1d} + \gamma_0$ proposed by [27–29]. Details of these equations can be found in an earlier publication [30], the intercept of each line with the P/d axis represents the surface energy γ_o. Figure 7 depicts the surface energy as a function of the plasma-processing time. From this figure, one can see that the value of the surface energy increases as the plasma-processing time increases. Directed cell adhesion remains an important goal of implant and tissue engineering technology. The ability to engineer directed cell responses to material surfaces is dependent upon a clear understanding of how different surface characteristics on various biomaterials affect implant–cell interactions. This understanding is a prerequisite for optimizing scaffolding and implant surface performance. Generally, the surface energy is proportional to cellular adhesion strength. Cellular adhesion on metals demonstrated a linear correlation with surface energy. Materials of higher surface energy have higher cellular adhesion [31].

According to Johnson [32] and Raaif *et al* [30], the main trend in the yield strength and Young's modulus in the nitrided layer of Ti–6Al–4V samples can be found. Figures 8 and 9 show the relative values of the yield strength and Young's modulus as a function of the applied load at different plasma-processing times, respectively. These figures show that the relative values of yield strength and Young's modulus decrease with increasing applied load for all the treated samples.

With the geometry of a Vickers indentation, the indentation depth, h, is related to the indentation diagonal, d, by [33]:

$$h = \frac{1}{2} d \frac{\tan 22^\circ}{\sqrt{2}}. \tag{2}$$

Figure 10 depicts the surface microhardness values of the untreated and treated Ti–6Al–4V samples as a function of the penetration depth. The microhardness values decrease as the penetration depth increases; this result agrees well with Bekir *et al* [34]. The hardness measurements carried out with higher applied loads show lower values as a result of relatively soft substrate effects.

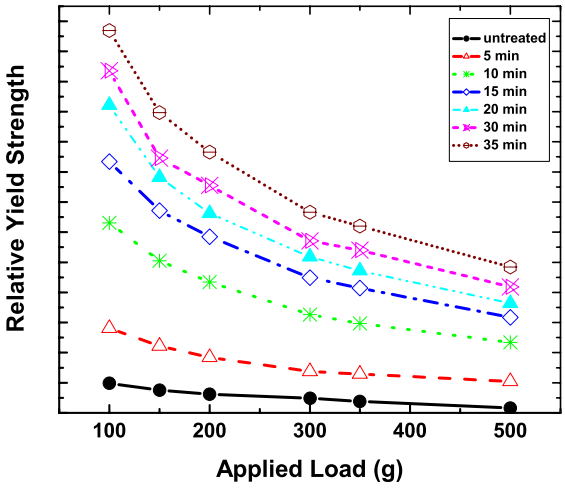

Figure 8. Relative yield strength of the untreated and treated Ti–6Al–4V samples as a function of the applied loads at different plasma-processing times.

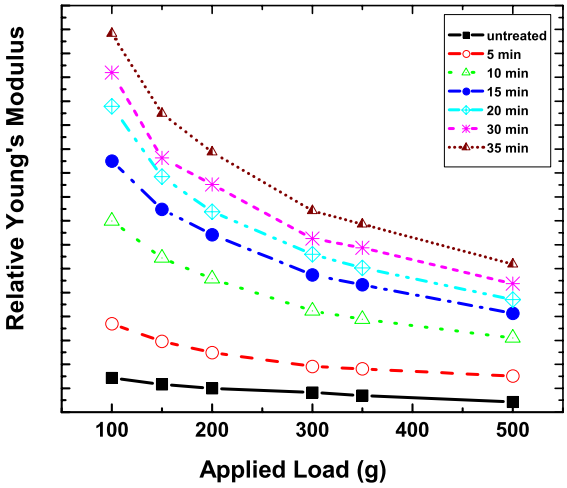

Figure 9. Relative Young's modulus of the untreated and treated Ti–6Al–4V samples as a function of the applied loads at different plasma-processing times.

The high microhardness value can be attributed to the high concentration of super-hard phases of TiN, Ti_2N, and Ti(N), which precipitated at the sample surface. The increase in surface energy is attributed to the formation of super-hard phases, which increases the surface microhardness and consequently the surface energy.

3.3. Surface roughness measurements

In the present study, the parameters root-mean square, R_q, and average roughness, R_a, were obtained using a Dektak3ST surface profile measuring system. The as-received Ti–6Al–4V was ground and polished to give an initial surface roughness R_a of 61 nm. Figure 11 shows the effect of the plasma-processing time on the surface roughness of the treated Ti–6Al–4V samples.

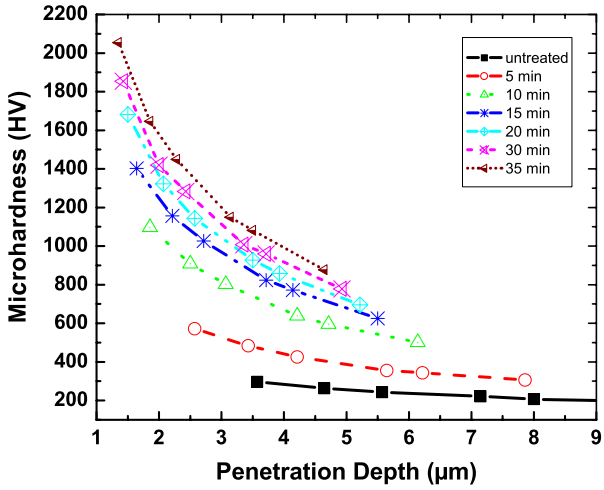

Figure 10. The variation of the microhardness values of untreated and treated Ti–6Al–4V samples using different plasma-processing times as a function of the penetration depth.

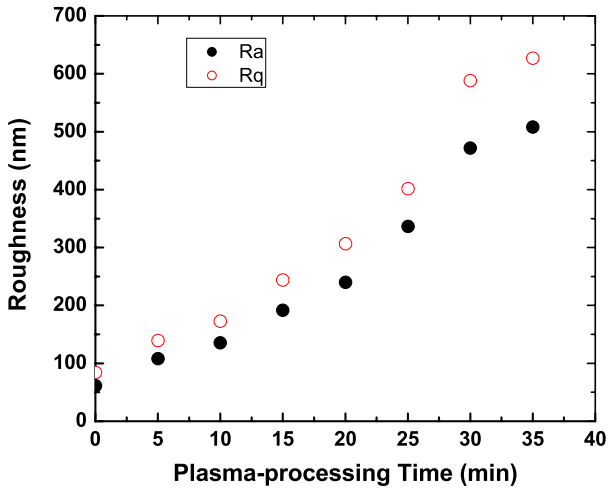

Figure 11. The surface roughness as a function of the plasma-processing time.

The values of R_a and R_q increase with increasing plasma-processing time. Blawert *et al* [35] have attributed the growth in surface roughness to the sputtering surfaces caused by ion bombardment during the treatment. Surface roughness can be divided into three levels depending on the use of biomaterial as an implant: macro-, micro- and nano-sized topologies. Surface profiles in the nanometer range play an important role in the adsorption of proteins, adhesion of osteoblastic cells, and thus the rate of osseointegration [36]. However, the optimal surface nano-topography for selective adsorption of proteins leading to the adhesion of osteoblastic cells and rapid bone apposition is unknown. A few strategies should be considered in order to improve both the short-and long-term osseointegration of titanium dental implants. These future trends concern the modifications of surface roughness at the nanoscale level for promoting protein adsorption and cell adhesion, biomimetic calcium phosphate coatings for

enhancing osteoconduction, and the incorporation of biological drugs for accelerating the bone healing process in the peri-implant area [37].

4. Conclusion

Inductively coupled rf-plasma nitriding has been used to modify the surface of Ti–6Al–4V. A high nitriding rate of 2.81 $\mu m^2\ s^{-1}$ was achieved. The surface microhardness increased from 297 to 2000 HV0.1 and the surface energy increased from 32.1 to 107.7 $N\ mm^{-1}$ by using high-efficiency plasma nitriding. The high concentration of nitrogen, the high reactivity of Ti–6Al–4V with nitrogen, and the formation of the super-hard phases TiN, Ti_2N, and Ti(N) are the reasons for these attractive properties.

Acknowledgment

I would like to thank the German Academic Exchange Service (DAAD) for awarding me a two-year dual-channel system grant through cooperation with the High Educational Ministry of Egypt.

References

[1] Nie X, Leyland A and Matthews A 2000 *Surf. Coat. Technol.* **125** 407
[2] Shenhar A, Gotman I, Radin S, Ducheyne P and Gutmanas E Y 2000 *Surf. Coat. Technol.* **126** 210
[3] Maa S, Xua K and Jieb W 2004 *Surf. Coat. Technol.* **185** 205–9
[4] Fouquet V, Pichon L, Drouet M and Straboni A 2004 *Appl. Surf. Sci.* **221** 248–58
[5] Yilbas B S, Sahin A Z, Al-Garni A Z, Said S A M, Ahmed Z, Abdulaleem B J and Sami M 1996 *Surf. Coat. Technol.* **80** 287–92
[6] Morita R, Azuma K, Inoue S, Miyano R, Takikawa H, Kobayashi A, Fujiwara E, Uchida H and Yatsuzuka M 2001 *Surf. Coat. Technol.* **136** 207–10
[7] Rie K-T, Stucky T, Silva R A, Leitaõ E, Bordji K, Jouzeau J-Y and Mainard D 1995 *Surf. Coat. Technol.* **74/75** 973–80
[8] Czarnowska E, Wierzchon T and Maranda-Niedbala A 1999 *J. Mater. Proc. Technol.* **92/93** 190–4
[9] Bars J-P, Etchessahar E and Debuigne J 1976 *CNRS RCP No. 244*
[10] Morita T, Takahashi H, Shimizu M and Kawasaki K 1997 *Fatigue Fract. Eng. Mater. Struct.* **20** 85–92
[11] El-Hossary F M, Negm N Z, Khalil S M and Raaif M 2005 *Appl. Surf. Sci.* **239** 142
[12] El-Hossary F M, Negm N Z, Khalil S M and Raaif M 2006 *Thin Solid Films* **497** 196–202
[13] El-Hossary F M, Negm N Z, Khalil S M and Abd Elrahman A M 2002 *Thin Solid Films* **405** 179
[14] Fedirko V M and Pogrelyuk I M 1983 *Sov. Mater. Sci.* **19** 511
[15] Maksimovich G G, Fedirko V M and Pogrelyuk I M 1987 *Sov. Mater. Sci.* **23** 566
[16] Maksimovich G G, Fedirko V M and Pogrelyuk I M 1988 *Sov. Mater. Sci.* **24** 611
[17] Metin E and Inal O T 1989 *Metall. Trans.* A **20** 1819
[18] Malinov S, Zhecheva A and Sha W 2003 *Proc. 1st Int. Surface Engineering Congress and the 13th IFHTSE Congress* (Materials Park, OH: ASM International) p 344
[19] El-Hossary F M 2002 *Surf. Coat. Technol.* **150** 177
[20] Man H C, Zhao N Q and Cui Z D 2005 *Surf. Coat. Technol.* **192** 341–6
[21] Conrad H 1982 *Prog. Mater. Sci.* **26** 123
[22] Barbieri F C, Otani C, Lepienski C M, Urruchi W I, Maciel H S and Petraconi G 2002 *Vacuum* **67** 457–61
[23] Taktak S and Akbulut H 2004 *Vacuum* **75** 247–59
[24] Kawata K, Sugimura H and Takai O 2001 *Thin Solids Films* **390** 64
[25] Leenders A, Ullrich M and Freyhardt H C 1997 *Physica* C **279** 173–80
[26] Veerender C, Dumke V R and Nagabhooshanam M 1994 *Phys. Status Solidi* a **144** 299
[27] Hirao K and Tomozawa M 1987 *J. Am. Ceram. Soc.* **70** 497
[28] Fröhlich F, Grau P and Grellmann W 1977 *Phys. Status Solidi* a **42** 79
[29] Frischat G H 1985 *Strength of Inorganic Glass* ed C R Kurkjian (New York: Plenum) p 135

[30] Raaif M, El-Hossary F M, Negm N Z, Khalil S M and Schaaf P 2007 *Appl. Phys.* A at press (doi:10.1007/s00339-007-4168-5)
[31] Hallab N J, Bundy K J, O'Connor K, Moses R L and Jacobs J J 2001 *Tissue Eng.* **7** (1)
[32] Johnson K L 1970 *J. Mech. Phys. Solids* **18** 115
[33] Jonsson B and Hogmark S 1984 *Thin Solids Films* **114** 257
[34] Yllbas B S, Sahin A Z, A1-Garni A Z, Said S A M, Ahmed Z, Abdulaleem B J and Sami M 1996 *Surf. Coat. Technol.* **80** 287–92
[35] Blawert C, Weisheit A, Mordike B L and Knoop F M 1996 *Surf. Coat. Technol.* **85** 15
[36] Brett P M *et al* 2004 Roughness response genes in osteoblasts *Bone* **35** 124–33
[37] Le Guéhennec L, Soueidan A, Layrolle P and Amouriq Y 2007 *Dental Mater.* **23** 844–54
[38] Holmgerg B 1962 *Acta Chem. Scand.* **16** 1255
[39] Lengauer W and Ettmayer P 1986 *J. Less-Common Met.* **120** 153
[40] Wong-Ng W, McMurdie H, Paretzkin B, Hubbard C and Dragoo A 1987 *ICDD Grant-in-Aid* (Gaithersburg, MD: NBS)
[41] Beattle J H and VerSnyder F 1953 *Trans, Am. Soc. Met.* **45** 397
[42] Lobier G and Marcon J P 1969 *Acad. Sci. Paris* **C268** 1132–35
[43] Becker K and Ebert F 1925 *Z. Phys.* **31** 269
[44] Lengauer 1986 *J. Less-Common Met.* **125** 127